# Convection; Significance for Stellar Structure and Evolution

Å. Nordlund[1,2] and R. .F. Stein[3]

[1]Theoretical Astrophysics Center, Copenhagen
[2]Astronomical Observatory / NBIfAFG, University of Copenhagen
[3]Dept. of Phys. and Astronomy, Michigan State University, East Lancing

**Abstract:** We present our current understanding of stellar convection based on the lessons that can be drawn from numerical convection simulations. We discuss properties of convection in the surface layers and in the bulk of the convection zone and we consider indirect effects of convection on stellar atmospheres. The average thermal properties of convection obtained from numerical simulations are very robust and are essentially unchanged as the resolution is increased. These thermal properties change extremely rapidly near the surface, on scales much smaller than the size of the convective cells transporting the energy. The interconnected downflow lanes visible as intergranule lanes at the solar surface quickly decompose into isolated downdrafts and the separation scale between these downdrafts gradually increases with increasing depth. A distinct asymmetry develops between the upflow and downflow regions because the ascending fluid flow is diverging and the descending flow converging in order to conserve mass. Most of the entropy fluctuations occur, most of the buoyancy work is performed, and most of the flux is transported, in the downdrafts. Penetration of downflows into the stable subconvective layers produce some entropy fluctuations, but these are smoothed out in the ascending gas over a few scale heights due the flow's divergence. Stellar convection is primarily driven by entropy fluctuations produced by radiative cooling at the surface. The lower part of the convection zone is slightly stably stratified, due to heating of the fluid by the radiative flux as energy transport gradually switches from radiative to convective.

Aside from its direct affect on stellar structure, convection also plays a significant role in controlling the structure of stellar atmospheres by driving the atmospheric dynamics. Convection excites the p-mode oscillations, generates waves that give rise to the enhanced chromospheric emission and stresses the magnetic field to supply energy to the corona.

## 1 Introduction

Convection is a key factor in stellar structure and evolution, both for obvious and direct reasons having to do with the strong constraint convection imposes on the thermal stratification, as well as for more indirect and less obvious reasons such as chemical mixing, angular momentum transport, magnetic dynamo action, surface activity, and stellar winds. These phenomena all ultimately have their origin in the convection zone dynamics, and through them, convection influences not only the evolution of the stars, but also the interaction of stars with the interstellar

"Stellar Evolution : What Should Be Done"; 32nd Liège Int. Astroph. Coll., 1995

medium.

In this paper, we summarize our present understanding of stellar convection. Much of the recent progress in the understanding of stellar convection has come through the use of supercomputer simulations. Both simulations of idealized setups, with ideal gases in models with impenetrable boundaries (Graham 1977; Chan & Sofia 1986, 1989; Toomre et al. 1990; Hossain & Mullan 1990, 1991; Cattaneo et al. 1991; Porter & Woodward 1994; Brummell et al. 1995; Hurlburt et al. 1995), and more realistic simulations, with equations of state that include atomic ionization and molecular dissociation, energy transport by radiation, and open upper and lower boundaries (Nordlund 1982, 1985, 1986; Gigas & Steffen 1984; Steffen et al. 1989; Steffen & Freytag 1991; Solanki et al. 1995; Stein & Nordlund 1989, 1991, 1994; Nordlund & Dravins 1990; Rast et al. 1993) have contributed to the qualitative understanding that we attempt to summarize briefly here.

First (section 2), we briefly outline current issues in the understanding of stellar (envelop) convection. Next (section 3), we discuss the crucial stellar surface layers, where convection is generally most violent, and where the transition from convective to radiative energy transport occurs. Then (section 4), we discuss convection on larger scales, up to and including global scales; i.e., motions on the scale of the entire convection zone. We also consider (section 5) the transition layer between the convection zone and the stably stratified layers below. Finally (section 6), we look at indirect influences of convection on the solar atmosphere.

## 2 Stellar Convection: Issues

The main uncertainties in stellar structure due to the influence of convection may be conveniently discussed with reference to Fig. 1. The distorted radius scale brings out the rapid

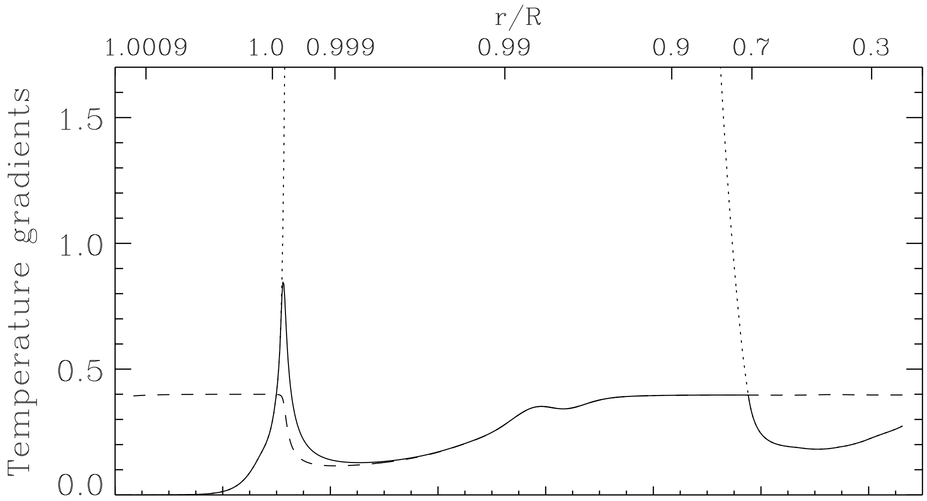


Figure 1: Logarithmic temperature gradients in a standard model of the solar convection zone (courtesy J. Christensen-Dalsgaard). The dashed line is the adiabatic temperature gradient, the dotted line is the radiative temperature gradient, and the full drawn one is the temperature gradient adopted in a local mixing length model.

variation of the convective instability with depth in the surface layers. It is the structure of the temperature gradient in a narrow surface region (a few tens of kilometers) that almost entirely determines the entropy in the bulk of the convection zone. The entropy is almost constant throughout most of the convection zone, and the equation of state is near that of an ideal gas, except in the regions of hydrogen and helium ionization close to the surface.

Some issues at the surface are: what determines the jump in entropy at the surface, how large are the deviations from hydrostatic equilibrium, how do these factors influence the interpretation of helio- and astero-seismology measurements of p-mode oscillations, and what excites these oscillations anyway?

In the bulk of the convection zone it is important to understand the structure and statistics of the flow, even if it is nearly adiabatic, in order to correctly assess the transport of for example angular momentum (Brandenburg et al. 1990; Pulkkinen et al. 1991; Pulkkinen et al. 1993) and magnetic fields (Nordlund et al. 1992; Brandenburg et al. 1995).

At the bottom of the convection zone, the main uncertainty lies in the undershoot of the convective motions beyond the point of marginal stability, and the consequence thereof for on the one hand the structure and on the other hand the diffusion of chemical elements (the lithium problem).

In addition to the scientific issues, there are also issues of a more practical and numerical character, such as how to treat the transonic flows near the surface, and how to deal with the enormous difference in density between the top and bottom of the convection zone, as well as with the differences in geometrical scales between the surface convection and convection at the scale of the full convection zone.

Figure 2 illustrates the range of scales involved in solar convection. It is obviously futile to attempt to cover the entire range of scales (both spatial and temporal) in one set of experiments. Instead, one may model the surface layers separately, if care is taken with the boundary conditions; open boundary conditions are required to avoid disastrous influence from (in particular) the lower boundary (Nordlund & Stein 1990; Nordlund et al. 1994).

Global scale models, on the other hand, cannot possibly include all the details of the surface layers. There, it is essential to emulate the influence of the surface layers, and to push the upper boundary as close to the surface as possible, while still maintaining numerical stability.

In the following sections we discuss surface layer models and global models separately.

# 3 Surface Layer Convection

The qualitative properties of convection in the surface layers of stars—and the generic difficulties associated with modeling these layers theoretically—are obvious already from a casual look at the structure predicted by one-dimensional, local theories such as the classical mixing length theory (Böhm-Vitense 1958) and the Canuto & Mazzitelli (1991) variant thereof. According to these estimates, the properties of convection change very rapidly just below the visible surface of stars such as the Sun.

Indeed, in these local models, the solar convection zone ends a few tens of kilometers above the surface of unit continuum optical depth. On the other hand, just a few tens of kilometers below the optical surface, these formula estimate convective velocities of several $\mathrm{kms}^{-1}$, and substantial temperature fluctuations. Even in terms of the cell sizes assumed in these theories (of the order of a pressure scale height, or a few hundred kilometers), the scale of variation is substantially smaller than the cell size, which violates the assumptions behind the theories.

## 3.1 Granulation

In the case of the Sun, the energy carrying convection cells are actually visible on the surface, as solar granulation. The sizes of the major energy carrying cells are of the order of 1000 -

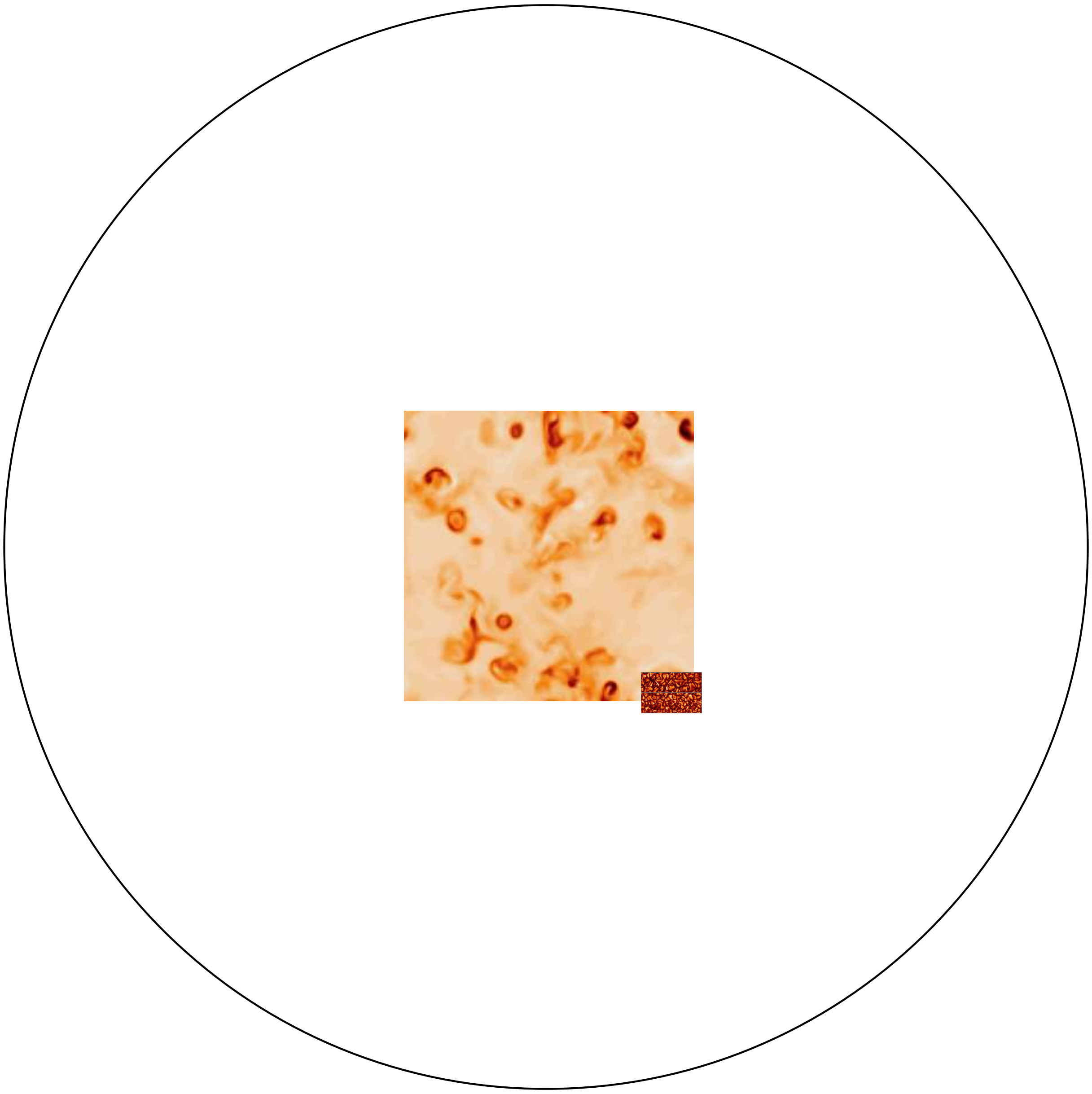

Figure 2: Convective scales in models of the solar convection zone. The large circle represents the Sun. The $400\times400$ Mm square shows the entropy in a horizontal plane at about half the depth of the convection zone, in a cartesian model with a 200 Mm deep convection zone sandwiched between stable layers below and above, with a radiative diffusion coefficient derived from a scaled Kramer opacity, but with a total flux of the order of $10^6$ times the solar value. The smaller square (real size $18\times12$ Mm) represents surface convection on granulation scales. It is shown at a slightly larger scale here.

3000 km, in contradiction to the assumptions behind mixing length theory and the Canuto & Mazzitelli (1991) formulae.

The scales of the dominant energy carrying cells are thus about two orders of magnitude larger than the scale of variation of the convectively unstable stratification, and about one order of magnitude larger than the density and pressure scale heights. The real convective motions do not stop at the optical surface of the Sun, but penetrate throughout the entire solar photosphere (whose thickness of about 500 km is still small compared to the horizontal scale of the convection cells). The density changes with over three orders of magnitude across this region. The energy balance (and hence the amount of stabilizing temperature fluctuations) is strongly influenced by radiative transfer effect such as spectral line "blanketing" in the upper photosphere.

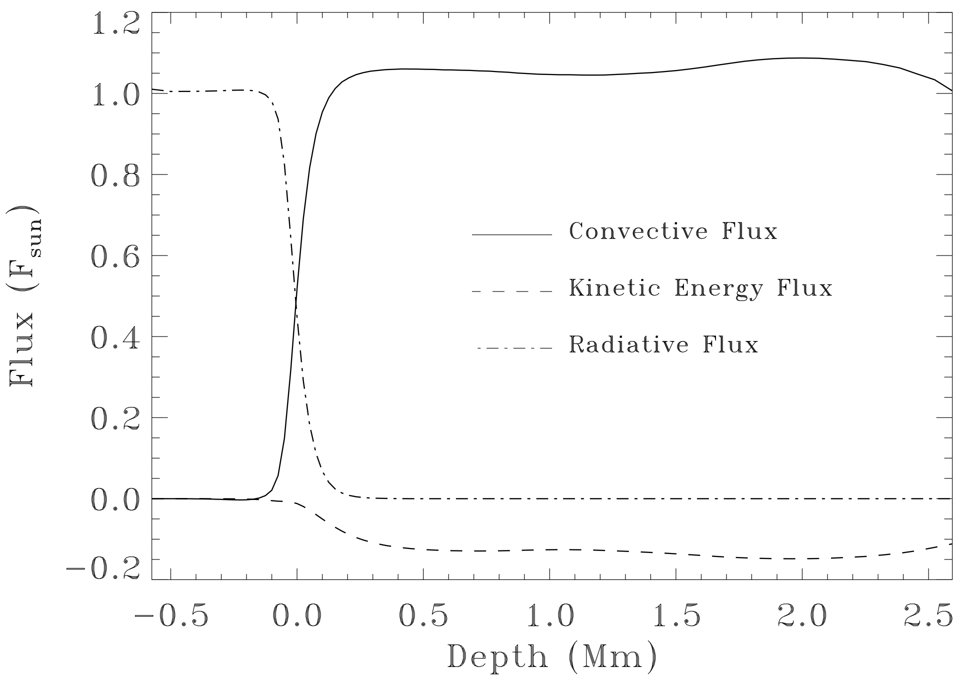


Figure 3: Horizontally and temporally averaged enthalpy, radiative and kinetic energy fluxes near the top of the convection zone. Note that the transition from convective to radiative energy transport at the solar surface is very abrupt. The kinetic energy flux is directed downwards (due to the highspeed downdrafts) and is about 10% of the enthalpy flux, which is larger than the solar value to compensate.

In addition to the rapid variation of the convective properties with height, other properties also change dramatically. The continuum absorption coefficient, for example, is dominated by $H^-$, which is proportional to the electron density. Because hydrogen is ionizing at temperatures around the solar surface temperature, the electron density is very sensitive to temperature changes. As a result, the mean opacity scales roughly as $T^{10}$. This is the main reason that the convective flux gives way to radiative flux so rapidly. Once the temperature starts dropping a few % (as a function of radius) near the surface, the opacity drops about ten times faster, which exposes the layer to significant radiative cooling, causing the temperature to drop even more.

The discussion applies in particular to ascending gas, but Fig. 3 shows that even the average convective flux has very sharp transition near the upper boundary. Note also that the kinetic energy flux is small relative to the convective flux. This is because the ionization causes a large specific heat capacity, and one can show that the ratio of convective to kinetic energy depends on the specific heat capacity (cf. Rast et al. 1993).

It is no coincidence that these effects all occur in the same layers. It is indeed the ionization of hydrogen that causes both the rapid increase of opacity with temperature, and a rapid drop of the adiabatic temperature gradient with depth. The two effects in combination determine the point of transition from convective stability to convective instability.

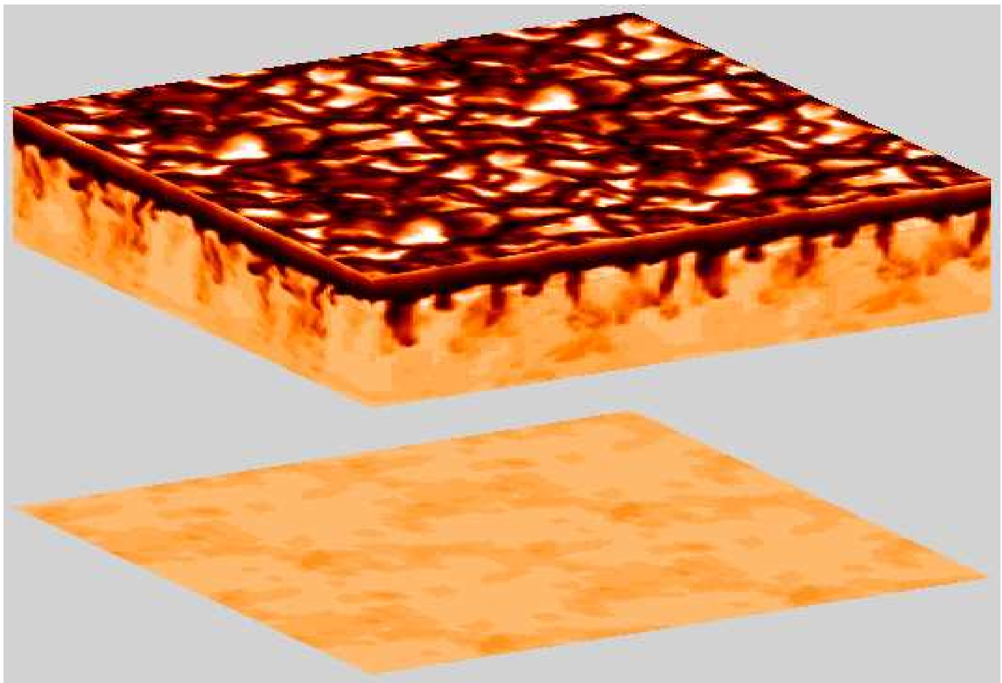

Figure 4: A perspective view of solar surface convection. The image on the top surface is the calculated optical surface brightness in a $12 \times 12 \times 9$ Mm model of solar surface convection (Stein & Nordlund 1996). The sides and the bottom plane (a plane at about 6 Mm depth, displaced vertically for viewing) shows the entropy. The weak larger scale pattern that may be discernible in the bottom plane is caused by larger scale (meso-granulation) flows that are not immediately visible at the surface).

It is obvious from the preceding discussion that it is in practice impossible to model the complicated surface region of a stellar convection zone with analytical models; a proper theory would have to include ionization effects, density stratification, convective overshoot, and multi wavelength radiative energy transfer. It is, however, straight forward to make numerical models of these surface layers. All of the effects mentioned above can be readily incorporated in numerical models, and with current supercomputer capacity one can afford sufficient numerical resolutions for a quite detailed modeling of stellar surface layers (cf. Fig. 4).

These numerical models are essentially parameter-free; apart from the numerical resolution (both in 3D space and in angles and frequencies involved in the radiative energy transfer) there are no tunable parameters (beyond the ones that define a stellar atmosphere; effective temperature, surface acceleration of gravity, and the chemical element abundances).

Our experience from solar modeling is that average quantities such as rms velocities, rms surface radiation intensities, and horizontal averages of thermodynamic quantities are extremely robust, and are essentially converged already at numerical resolutions of the order of $64^3$. Higher resolution is of course necessary to resolve finer details, such as for example the small scale details of the solar granulation (Fig. 5).

The quantitative agreement of synthesized optical diagnostics with both high resolution surface observations (Stein & Nordlund 1994 and see Fig. 5) and with spatially averaged spectral line profiles (Nordlund 1985a; Nordlund 1985b), and the robustness of the numerical results when the numerical resolution is increased renders a high degree of confidence to these models.

The convective motions are turbulent, albeit strongly influenced by the vertical density stratification. A short turbulent inertial range is discernible in two-dimensional (horizontal)

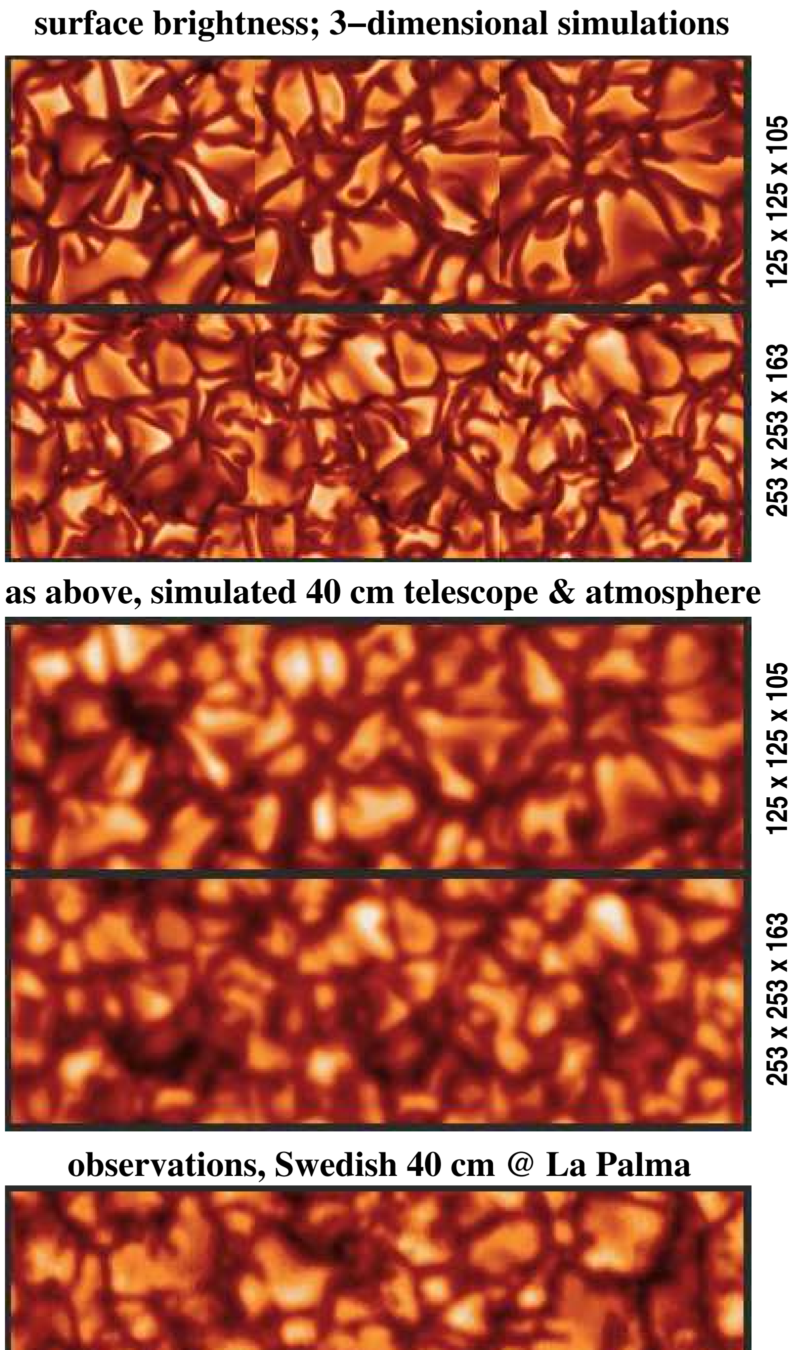


Figure 5: Synthetic images from models of the solar surface region, based on calculated surface brightness (in the continuum at 5000 Å), compared with high resolution observations from the Swedish Solar Observatory on La Palma (courtesy Bruce Lites and G. Scharmer). The upper two panels are as calculated from the models, the middle two are application of a point spread function (PSF) that represents the combined effects of the atmosphere and the instrument. This PSF reduces the intensity and Doppler velocity fluctuations to the same amplitude as in the observations. The size of each panel is approximately $18 \times 6$ Mm.

power spectra. With increasing numerical resolution, the extent of the inertial range increases correspondingly. This is also reflected in a decrease of the Taylor micro scale, and in a corresponding increase in the maximum value of the vorticity magnitude.

The scale and properties of the energy carrying motions change only marginally as the numerical resolution is increased, and the characteristic topology, with narrow, filamentary downdrafts, against an almost isentropic, slowly ascending background (Stein & Nordlund 1989) remains. The main changes come in increased small scale detail in the surface cell structure, and in increased turbulence in the subsurface downdrafts.

The cell scale may indeed be understood as a simple consequence of mass conservation; with horizontal scales characterized by wave numbers $k_x = k_y = k_{\mathrm{horizontal}} = 2\pi/\lambda_{\mathrm{horizontal}}$, and an exponentially decreasing mass flux $\rho\vec{u}$ with scale height $H_{\mathrm{horizontal}}$, one obtains from the continuity equation

$$4\pi k_{\mathrm{horizontal}} \approx 1/H_{\mathrm{vertical}}, \tag{1}$$

which explains why the horizontal scales are about an order of magnitude larger than the density scale heights.

Earlier experience with anelastic models (Nordlund & Dravins 1990), and recent experience with fully compressible models (Trampedach et al. 1996) show that the overall structure remains similar in other stars, and that surface cell sizes indeed scale roughly as the scale height in the photosphere.

## 3.2 The Role of the Turbulent Pressure

The motions in the solar surface layers are mostly subsonic, but with occasional supersonic motions (Cattaneo et al. 1990; Nordlund & Stein 1991). The turbulent pressure $P_{\mathrm{turb}} = \langle \rho u_z^2 \rangle$ is large enough to influence the stratification noticeably in the surface layers, where the additional support from $P_{\mathrm{turb}}$ elevates the surface about 35 km, relative to a similar model in hydrostatic equilibrium.

In giant stars the convective velocities are higher, and hence this effect is enhanced. Even in a sub-giant such as $\eta$–Boo, where p-modes were recently detected (see Christensen-Dalsgaard et al. 1995), the effect is quite significant; the photosphere is elevated more than two pressure scale heights. The motions in the photosphere of $\eta$–Boo may be characterized as "fountain flows"; i.e., the upwelling granule gas almost free-falls from the photosphere back into the denser layers.

Analysis of the effects of the structure difference between 3D models and standard 1D models (Stein & Nordlund 1991; Rosenthal et al. 1995) shows that the changes associated with the turbulent pressure is the main reason for the discrepancy between the observed p-mode frequencies and those calculated from standard 1D models. Part of the effect comes from the elevation, part from the influence of the turbulent pressure on the effective $\Gamma_1 = \left(\frac{\partial \ln P}{\partial \ln \rho}\right)_S$.

# 4 The Bulk of the Convection Zone

Even from the very first, low resolution models (Nordlund 1982), it was obvious that the topology of the flow beneath the surface is different from the cellular pattern that is so distinct at the surface. The bright cells, surrounded by a connected dark pattern gives way to a rather structureless homogeneous background, with intermittent patches of cold, descending material. Using tracer particles, Stein & Nordlund (1989) showed that this transition—that happens on a scale much *smaller* than the surface cell size—occurs because all cooling takes place at the surface. It is only at the surface that all overturning gas is exposed to cooling, and hence arrives at the intercellular lanes with a lower entropy. Below the surface, the only cooling that occurs is indirect, and caused by mixing with fluid that has recently been at the surface. Since the cool intercellular gas rapidly drains into the vertices between cells, a transition occurs to horizontal planes with patchy spots of cool gas.

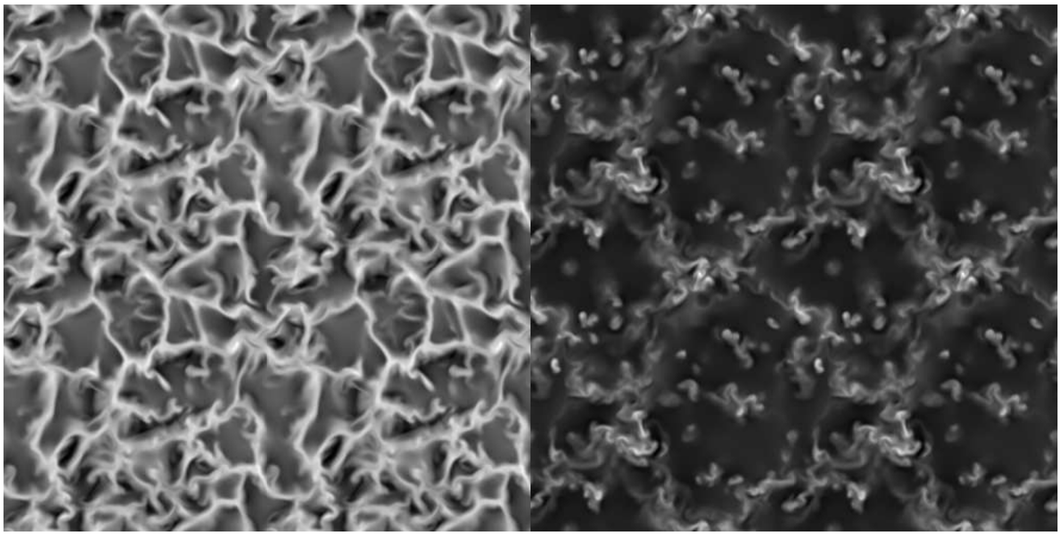

Figure 6: Vertical velocity at the surface (left) and 1 Mm below it (right). Light areas are downflows and dark areas are upflows. The scale is 12 Mm on a side and the computational domain has been doubled in each direction to more clearly reveal the large scale structure. Note that the scale of the cells has dramatically increased 1 Mm below the surface, yet the downflows are still confined to narrow lanes.

A more gradual transition in the cell size occurs further down below the surface. Because of the rapidly increasing density scale height, the horizontal sizes allowed by Eq. (1) increase correspondingly. Semi-cellular patterns of increasing size are supported at larger depths, as the overturning motions on larger and larger scales sweep the smaller scale patterns sideways into intercellular “lanes”. These “lanes” are more patchy than the lanes at the surface, reflecting the pseudo-random mapping of cool surface gas onto deeper lying horizontal planes (cf. Fig. 6). Equation (1) implies that we may expect the dominant horizontal scales to reach global scales at depths of less than 100 Mm.

The mapping from one plane to another is strongly influenced by the density stratification. Consider not just the order of magnitude of the terms in the continuity equation, as in Eq. (1), but the signs as well. It is obvious that $\partial(\rho u_z)/\partial z$ is on the average positive in descending gas and negative in ascending gas. Hence, because the horizontal mass flux divergence $\partial(\rho u_x)/\partial x + \partial(\rho u_y)/\partial y$ must, on the average, balance the vertical one, the horizontal flow is converging in descending gas and diverging in ascending gas. This is similar to the convergence and divergence of horizontal flows near the boundaries of incompressible fluids, but here the situation extends throughout most of the convection zone, because of the density stratification.

The systematic horizontal convergence of downdrafts and divergence of updrafts has profound consequences, since it introduces a fundamental asymmetry between up and down. For example; all patterns in downdraft regions tend to shrink in size, while all patterns in updrafts tend to expand. One consequence of this is that turbulence is much easier to maintain in the downdrafts, where patches of cool gas (and hence buoyancy work) tends to concentrate. A related consequence is that the vertical momentum itself, and the kinetic energy, tend to concentrate in the downdraft regions, thus creating a marked asymmetry between upflows and downflows. Figure 7 illustrates the strong intermittency of the kinetic energy.

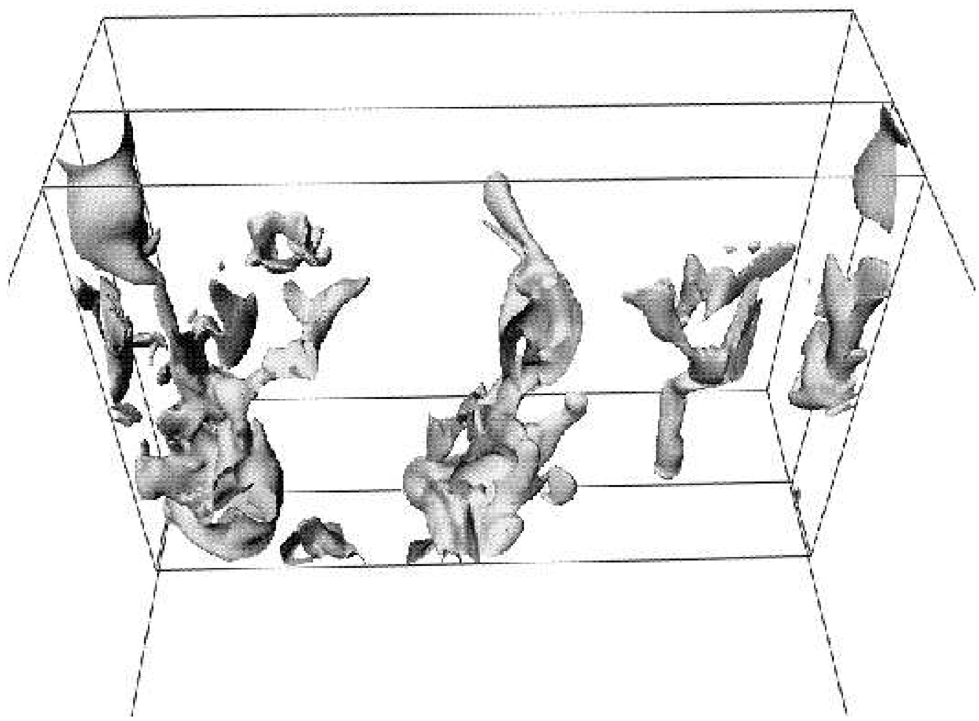

Figure 7: The kinetic energy density in a $12 \times 12 \times 9$ Mm model of convection in the solar surface layers. The kinetic energy density has been normalized with the horizontal rms value at each depth. An isosurface at 5% of the maximum energy density is shown, in a slice of about 1.5 Mm thickness. The volume fraction enclosed by this isosurface is only about 6%, demonstrating the high degree of intermittency.

## 4.1 Simulations of Global Scale Convection

Nordlund et al. (1994) demonstrated the importance of using a sufficient number of scale heights in the simulations, and the importance of not using an impenetrable lower boundary in the unstable layer. In models with a hard lower boundary, and with too few scale heights of stratification, the ratio of entropy fluctuations generated at the lower and upper boundaries will be incorrect.

The main factor here is the huge density stratification of the solar convection zone (with a density ratio of around $10^7$ from the photosphere to the bottom of the convection zone). Thus, there has to be an enormous dilution of the cold, descending gas from the surface, before it reaches the bottom of the convection zone. On the other hand the only significant source of cooling is the surface boundary. Overshooting at the lower boundary introduces some cooling of overturning gas there, but the corresponding potential temperature fluctuations (the temperature fluctuations it would correspond to at the surface pressure) are only a few K. Entropy fluctuations injected into the ascending gas at the lower boundary are rapidly wiped out, because of the general expansion of the ascending flow.

We have set up a series of numerical experiments to model global scale convection, including the undershoot at the bottom of the convection zone (Nordlund et al. 1996). These models are, in contrast to the surface layer models discussed in Section 3, "toy models"; i.e., they are not designed to be accurate representations of, for example, the real solar convection zone. Such models are very difficult to construct, first of all because of the huge difference between the thermal (Kelvin-Helmholtz) time scale and the dynamic time scale (sound travel time).

To circumvent this difficulty, we model a convection zone with about $10^6$ times larger convective flux, relative to the solar one (we increase the cooling rate at the surface accordingly). From the scaling properties of the Navier-Stokes equations we expect that this exaggerates the convective velocities with a factor of $10^2$, but that the flow structures are otherwise similar. In order to model the transition from radiative to convective flux as realistically as possible, we include radiative diffusion, with a diffusion coefficient derived from Kramer's opacity law (again enhanced by a factor of $10^6$).

With this procedure, we expect to obtain a qualitatively correct behavior in the lower parts of the convection zone, where the radiative flux gradually diminishes from 100% to a very small value. This transition is simply a consequence of the logarithmic temperature gradient $\partial \ln T/\partial \ln P$ being very close to 2/5 (efficient convection in a fully ionized gas). The increase of Kramers opacity with falling temperature then dictates the profile $F_{\rm rad}(r)$.

# 5 Undershoot and Mixing

The exaggeration of the convective velocities leads to an exaggerated convective undershoot layer, below the convection zone proper (defined as the region where $F_{\rm conv}$ is negative). One important objective that we have is to find out how to scale the undershoot properties down to correct solar / stellar fluxes, to thus be able to estimate the effect of convective undershoot on chemical mixing.

In the classical undershoot layer, the convective flux is negative because descending fluid penetrates into a stable layer and hence finds itself being hotter than the average surroundings. However, above this undershoot layer, there is an extended region where the stratification is nominally stable (the entropy is increasing with radius), but where the convective flux is still positive (cf. Fig. 8). The reason for this is the gradual change in radiative flux.

The temperature gradient is "locked" to the adiabatic gradient everywhere that a deviation would force a significant convective flux divergence. This holds true through most of the convection zone, and it is only in the two boundary layers that the temperature gradient deviates noticeably from the adiabat. At the point where the convective (plus kinetic) energy flux passes through zero, the radiative flux passes 100% of the nominal solar flux. As one progresses to layers with lower temperature and pressure, the Kramer opacity increases gradually, and hence the radiative flux decreases. Throughout this region, there is a systematic and evenly distributed heating of both ascending and descending gas.

As a consequence, the entropy of the ascending gas increases with height, while the entropy of descending gas increases with depth (the entropy of descending gas also increases due to entrainment). The net effect, given the relative intermittency of the cool, descending gas, is that the average entropy increases with radius over a substantial fraction of the lower half of the convection zone. These layers are thus formally convectively stable. On the other hand (most of) the descending gas remains cooler than the average throughout these layers, and hence buoyancy work is still being performed on the convective flows in these layers.

The entrainment and reheating of descending gas may also be illustrated by displaying a two-dimensional histogram of the entropy, Fig. 9. The figure illustrates how the entropy contrast decreases with depth, that the median entropy (maximum brightness) decreases slightly with depth in the lower convection zone, while the minimum entropy (corresponding to the coolest

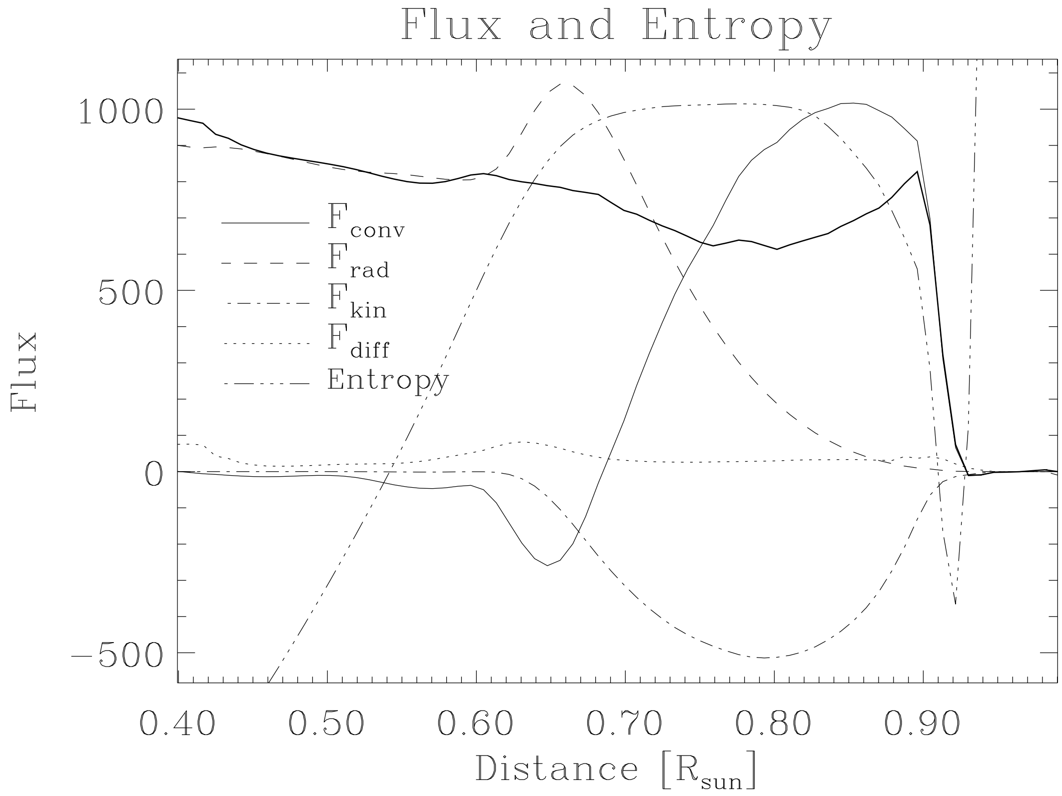


Figure 8: Convective, radiative, kinetic energy and viscous fluxes plus the net total flux and the entropy per unit mass. The entropy is nearly constant throughout the convection zone, but has a slightly stable gradient in the lower part of the zone, where the radiative flux is gradually decreasing and heating the gas as the Kramer's opacity increases with decreasing temperature. Near the top of the convection zone most of the flux is carried by the enthalpy or convective flux. Below the convective layer the convective flux becomes negative (transports energy downward) and the radiative flux becomes larger than the total net flux to compensate.

downdrafts) keeps increasing down to the bottom of the convection zone proper. Note the large difference in entropy contrast between the top and bottom of the model. The difference is still much less than in the real Sun, because our upper boundary is at some depth below the real surface.

Fig. 9 thus illustrates that the entropy fluctuations injected into the ascending flow at the bottom of the convection zone are much smaller than the ones injected at the top. Since entropy fluctuations in the ascending gas are rapidly washed out by horizontal expansion, it is clear why the picture in the bulk of the convection zone is one with intermittent patches of cold descending gas, against a smooth background of ascending gas. In this respect, solar convection resembles convection in the Earth's oceans, with descending thermals because in both cases the entropy fluctuations are produced at the upper boundary. The Earth's atmosphere, on the other hand, has rising thermals because it is primarily heated from below.

Figure 10 illustrates the overall situation. The vertical plane shown here goes through one of the few ($\approx$ 2–3) penetrating downdrafts that exist at any one time in our model (which is $400 \times 400$ Mm horizontally). In this particular vertical plane one can see the downdraft penetrating into the stable layer, spreading out a bit, and injecting a return flow back into the convection zone. The entropy of the return flow is mostly similar to that in the convection

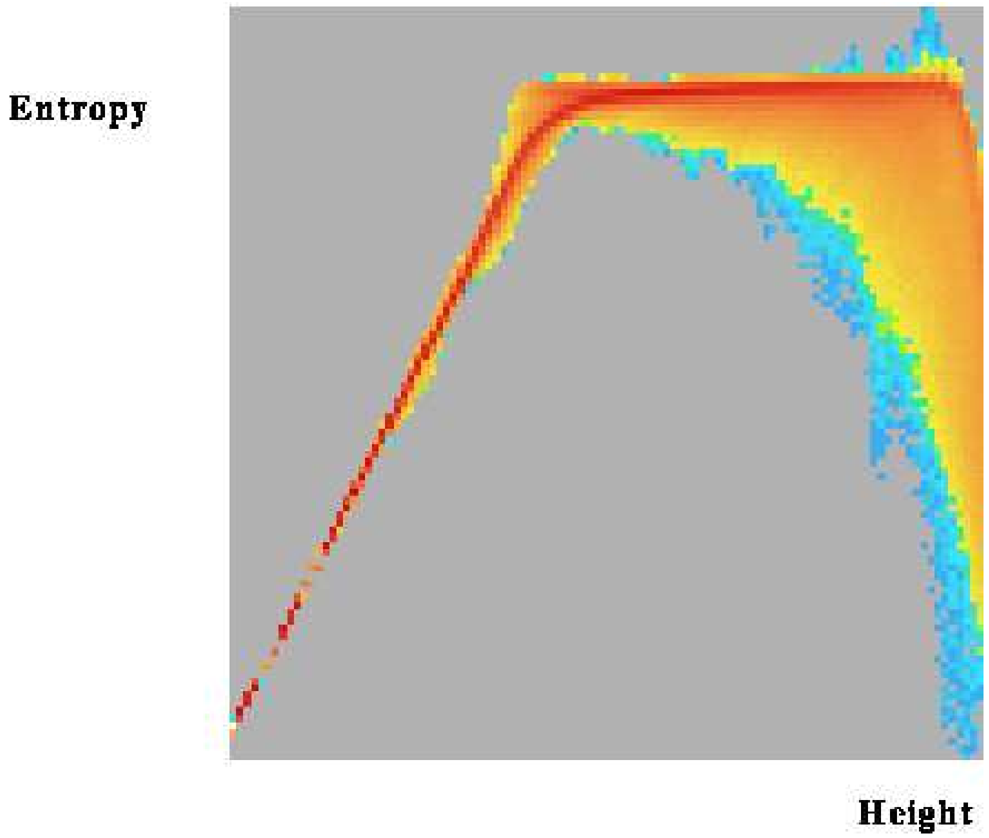


Figure 9: A two-dimensional histogram of entropy. Each pixel column is the probability distribution function (PDF) of entropy at given radius.

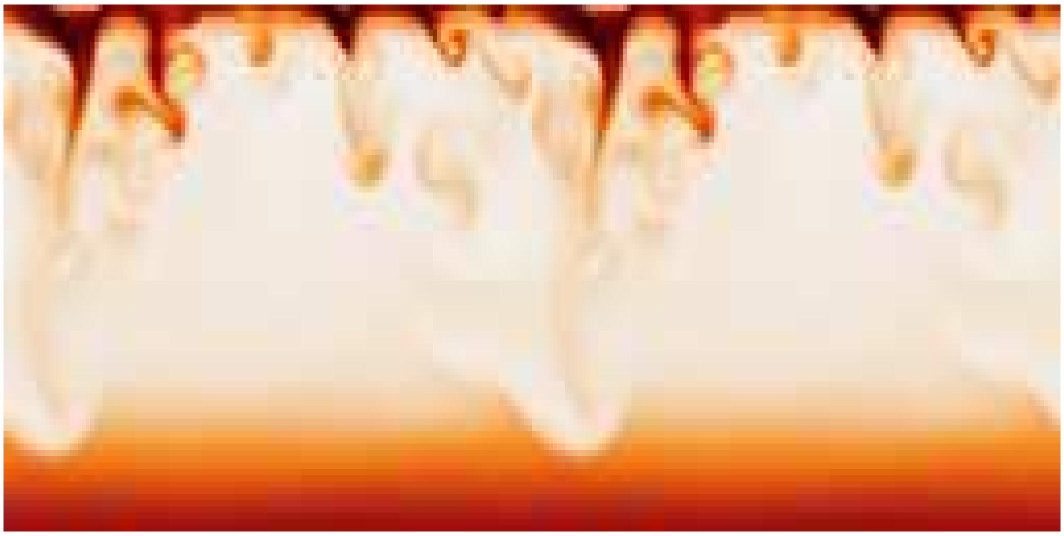

Figure 10: The entropy in a $400 \times 400 \times 350$ Mm "toy-model" of the solar convection zone (only about 220 Mm is shown vertically). The model is Cartesian instead of spherical, and the flux is about $10^6$ times solar, but the radial profile of radiative diffusion is roughly proportional to the solar one (a scaled version of Kramers opacity is being used), and the vertical density and pressure stratification are similar to solar. The overall extent of the model, including boundary layers and stable layers not shown here, is about 14 pressure scale heights.

zone; only a thin layer on the outside is subject to cooling by thermal diffusion.

Beyond the point where the descending gas becomes (on the average) warmer than the ascending gas, the buoyancy work becomes negative, and the descent is quickly stopped. In this region the correlation between vertical velocity and entropy fluctuations is negative, the convective flux is negative, and hence the radiative flux is larger than 100%. The point where the radiative flux passes through 100% is actually displaced upwards relative to the point where the convective flux changes sign, because of the kinetic energy flux. This kinetic energy flux is systematically negative (downwards) in most of the convection zone, because of the concentrated downdrafts.

Further down in the stable layers, the convective flux quickly becomes very small, but there are still significant motions. These are mainly waves, excited by the overshooting motions. As already emphasized earlier, the overall amplitudes of the motions in the convection zone are about two orders of magnitude too large in this “toy model”, as compared to those of the real sun. The wave motions, however, are exaggerated with a larger factor than the convective motions. If the excitation mechanism is mainly of a dipolar nature, one should expect the factor to be of the order of $10^4$, while if it was quadrupolar, it would be of the order $10^8$. We expect to be able to establish the scaling by repeating the experiments with different flux enhancement factors.

# 6 Indirect Influence

Convection excites the p-mode oscillations (Goldreich & Keeley 1977; Stein & Nordlund 1991; Goldreich & Kumar 1990) and drives waves into the solar chromosphere. The dynamic state of the solar atmosphere is very different from its average state. Acoustic waves propagating up through magnetic field free regions produce enhanced emission that has been interpreted as a semi-empirical chromospheric temperature rise. In reality, the mean temperature remains close to its radiative equilibrium value. The observed enhanced emission is produced by waves that generate short intervals of high temperatures, without any increase in the average gas temperature. Because of the temperature sensitivity of the source function in the ultraviolet, the radiation temperature represents preponderantly the peaks in the gas temperature rather than its mean (Carlsson & Stein 1995).

Waves with periods near 3 minutes, but modulated by both higher and lower frequency waves, form shocks near 1 Mm above the visible surface which produces the brightenings observed on the violet side of the H and K lines of ionized calcium (so called $H_{2V}$ and $K_{2V}$ bright grains). Shocks that occur at small enough heights that the line source function is still coupled to local conditions enhance the source function. The brightness of the violet peak depends on the shock strength and its height of formation; higher densities at lower heights produce stronger emission. The asymmetry in the line profile is due to the velocity gradient across the shocks. Emission is increased where there is large opacity at a small optical depth. An upward propagating shock accelerates the atoms, which Doppler shifts the frequency at which they absorb and emit photons to the violet side of the line. At these frequencies, offset from line center, there is little optical depth from the overlying material, which is general falling downward and absorbing and emitting photons on the red side of line center. Carlsson & Stein (1994) have simulated this process by driving waves through a radiative equilibrium atmosphere with a velocity chosen to match Doppler shifts in the iron line at 396.68 nm measured by (Lites et al. 1993). Figure 11 shows the excellent agreement obtained between the calculated and observed grains.

The convection zone is also the ultimate driver of coronal activity. The motions in the

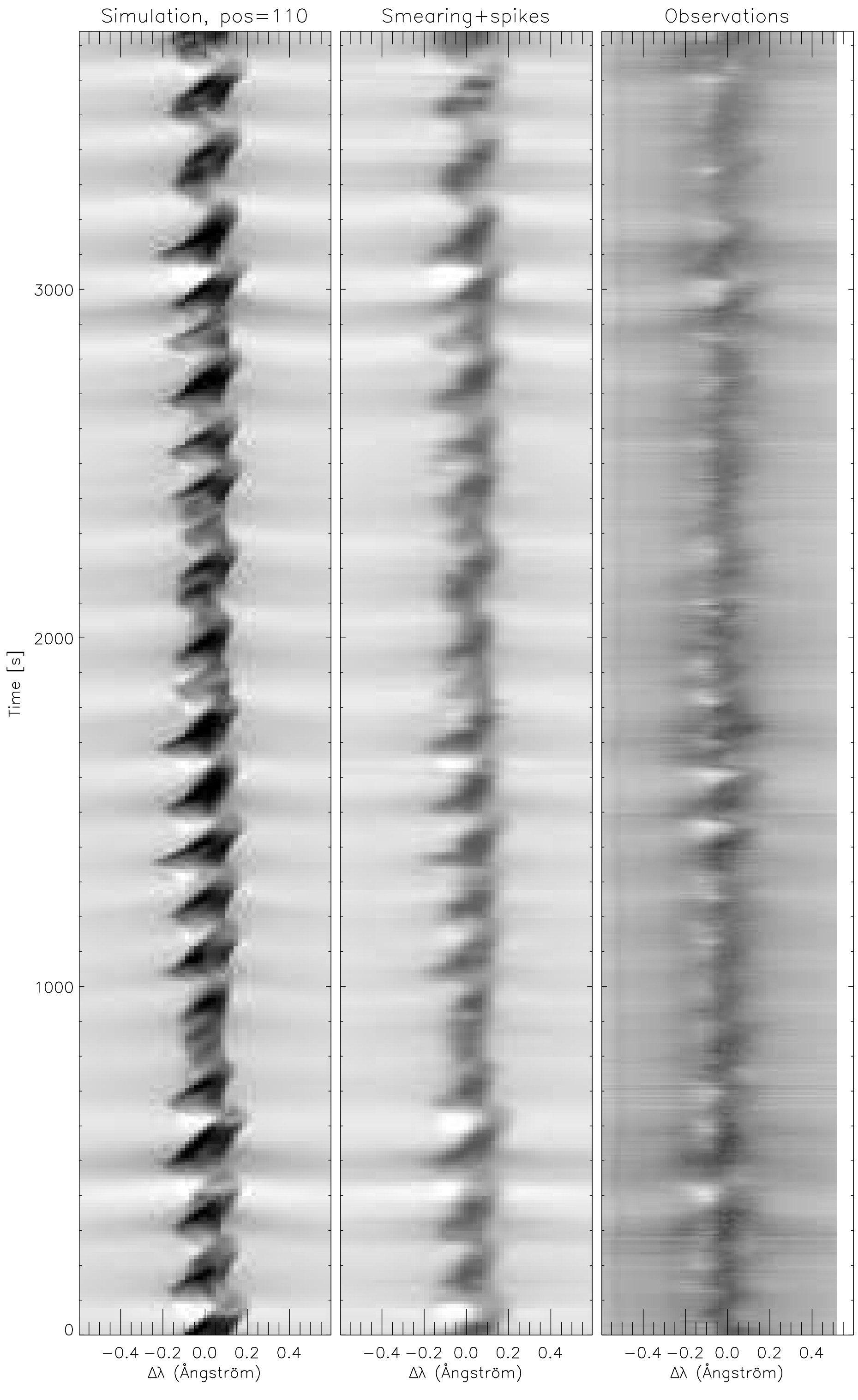


Figure 11: The computed CaII H line intensity as a function of wavelength and time compared with observations. The left panel shows the raw simulation results. The middle panel shows the simulated intensities convolved with a Gaussian point spread function with FWHM of 20 s in the time domain and 5 km/s in the wavelength domain. Scattered light amounting to 1% of the continuum intensity has been added. The image has also been shifted randomly in time to represent image motion. The right panel shows the observations. Note the close agreement in occurance and appearance of bright grains. The contrast is, however, larger in the simulation.

convection zone do work on the coronal magnetic field, by moving its foot points around. This generates a Poynting flux through the photosphere, corresponding to the work that the motion has to do on inclined field lines. Galsgaard & Nordlund (1995a) performed a series of experiments aimed at obtaining a qualitative understanding of dissipation in magnetically dominated plasmas, driven by shearing motions on two opposing boundaries. The set-up is a schematic representation of conditions in the solar corona. The results from these numerical experiments show that the dissipation of the imposed work takes place in a set of spatially complex, thin current sheets (cf. Fig. 12).

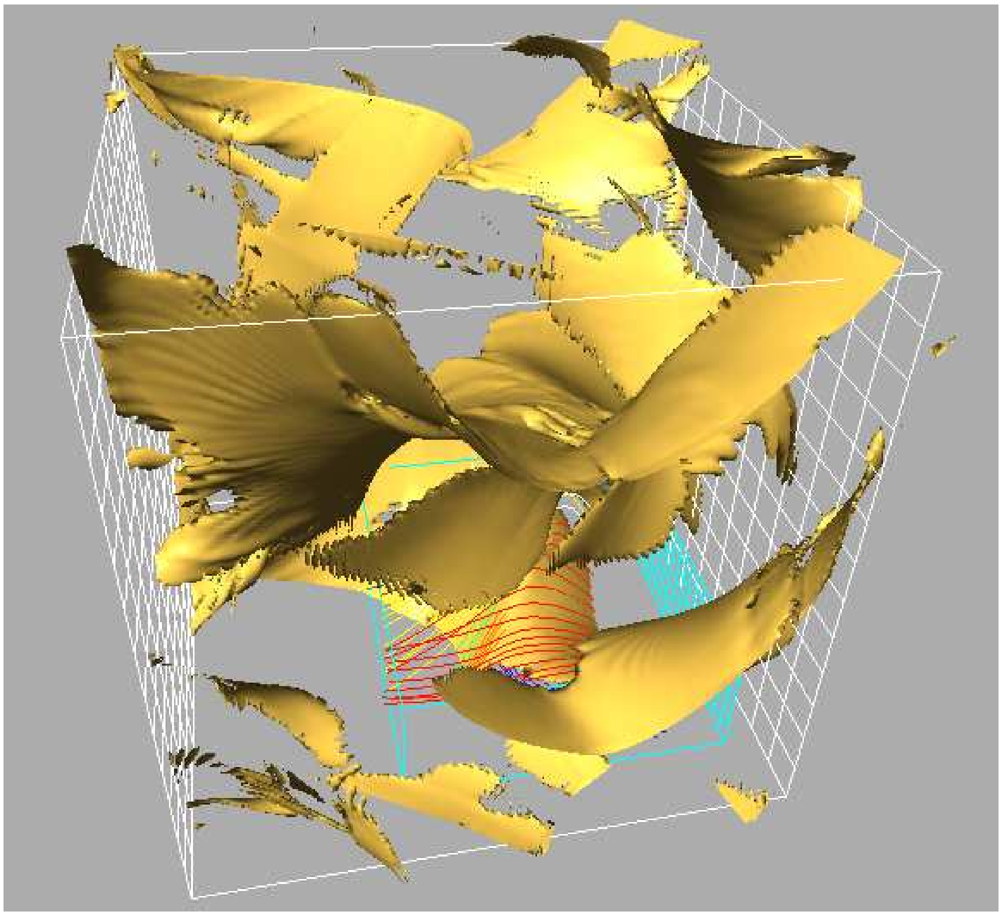

Figure 12: Current sheets, and the corresponding discontinuities in magnetic field line directions, in a simulation of a magnetically dominated plasma driven by material shearing motions on two boundaries (left and right). The isosurfaces show current sheets; thin structures with very high electrical current density. The direction of magnetic field lines is discontinuous across these surfaces.

For certain initial initial conditions and boundary conditions, the current sheets form an arcade-like structure anchored at one of the boundaries (Fig. 13).

The order of magnitude of the average dissipation is consistent with empirical estimates of the average coronal heating rate. The dissipation is quite intermittent in both time and space. This type of "DC"-stressing of the solar corona is therefore an excellent candidate both for providing the average coronal heating, as well as for building up the stresses that eventually lead to solar flares. Higher resolution numerical experiments will be needed to decide if the statistics of energy release in the numerical models will be able to match the observed power law distributions (Lu & Hamilton 1991; Lu et al. 1993; Lee et al. 1993; Galsgaard 1995).

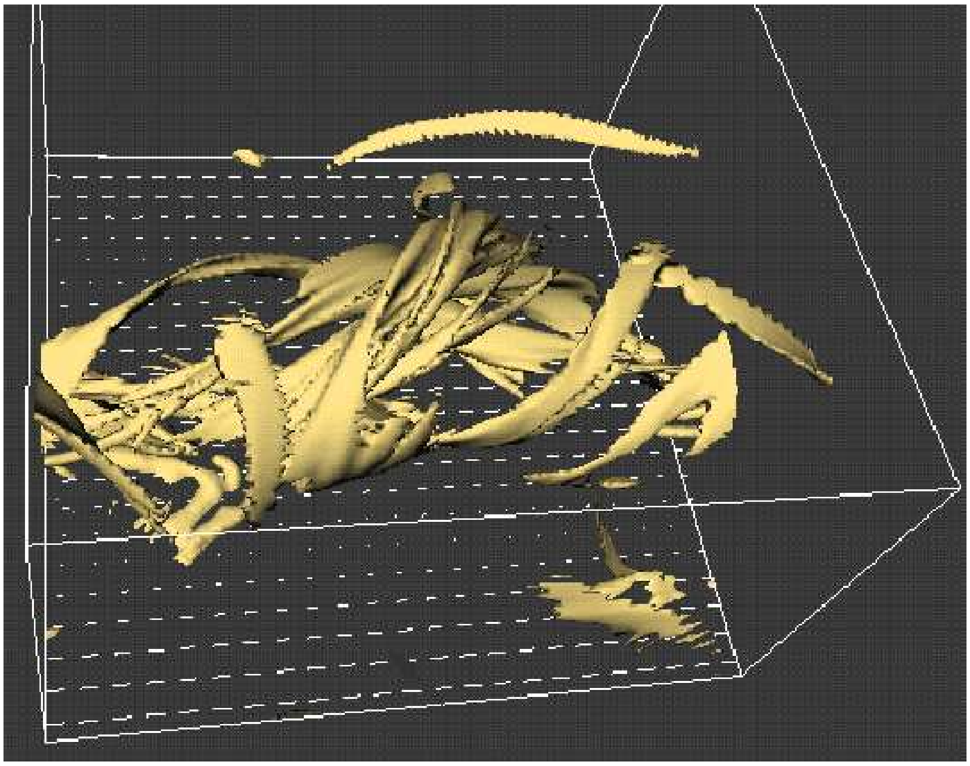

Figure 13: Isosurfaces of strong electric current in a simulation of a magnetically dominated plasma that initially contained eight null points. Large scale shearing of the boundary planes (the boundary shear pattern is indicated with arrows) have caused reconnection into a topology with an arcade-like structure along one of the driving boundaries (Galsgaard & Nordlund 1995b).

## 7 Conclusions

From a number of series of numerical experiments we conclude that supercomputer models of solar and stellar convection zones, and various aspects of their interaction with the surroundings—emission of radiation at the surface, excitation of global p-modes and g-modes, dynamo action and the associated emergence of active regions, as well as the dynamics of the chromosphere and corona—are very useful tools when seeking a qualitative understanding of such phenomena.

Many average aspects of these models are already converged at fairly small numerical resolutions, while others require numerical resolutions at and beyond the limits of current supercomputers. Futures simulations should aim, on the one hand, at complementing and matching the increasing wealth of observational information from projects such as GONG and SOHO, but also at investigating aspects that are not directly accessible to observations. Several aspects of the solar dynamo, for example, may be extremely difficult to obtain information about observationally, but may be amenable to computer simulations. The fine scale structure of the presumed strong toroidal magnetic field in the overshoot layer is one such example.

Global models of the solar dynamo may be one example where even the largest computers of the current generation are not sufficient for a brute force attack. Instead, one should aim at obtaining a qualitative understanding of subprocesses out of which a global scenario may be constructed.

Even global models of the solar convection zone are still out of reach, and may be so for quite some time, because of the very disparate time scales involved. In the mean time, we may systematically improve our understanding of the solar and stellar convection zones by building increasingly sophisticated "toy models".

Eventually, however, the exponential growth of computer capacity will catch up with the scenario building, and it will become possible to put the qualitative scenarios to more quantitative tests.

## Acknowledgements

The work of Å.N. was supported in part by the Danish Research Foundation, through its establishment of the Theoretical Astrophysics Center (TAC). R.F.S. was supported in part by NASA grants NAGW 1695, NAG 5-2218 and NAG 5-2489. The calculations were performed at the National Center for Supercomputer Applications, which is supported by the National Science Foundation, and at the UNI•C computing center in Copenhagen under a grant to TAC from the Danish Natural Science Research Council. Additional computing was done at the Centre National de Calcul Parallele en Sciences de la Terre in France.

## References

Böhm-Vitense, E. 1958, Zs. f. Ap., 46, 108
Brandenburg, A., Jennings, R. L., Nordlund, A., Rieutord, M., Stein, R. F., Tuominen, I. 1995, J. of Fluid Mech., (in press)
Brandenburg, A., Nordlund, Å., P., P., Stein, R. F., Touminen, I. 1990, A&A, 232, 277
Brummell, N. H., Hurlburt, N. E., Toomre, J. 1995, ApJ, (submitted)
Canuto, V. M., Mazzitelli, I. 1991, ApJ, 370, 295
Carlsson, M., Stein, R. F. 1994, in M. Carlsson (ed.), Chromospheric Dynamics, Proc. Mini-Workshop on Chromospheric Dynamics, Institute of Theoretical Astrophysics, Oslo, p. 47
Carlsson, M., Stein, R. F. 1995, ApJ, 440, L29
Cattaneo, F., Brummell, N. H., Toomre, J., Malagoli, A., Hurlburt, N. A. 1991, ApJ, 370, 282
Cattaneo, F., Hurlburt, N., Toomre, J. 1990, ApJ, 349, L63
Chan, K. L., Sofia, S. 1986, ApJ, 307, 222
Chan, K. L., Sofia, S. 1989, ApJ, 336, 1022
Christensen-Dalsgaard, J., Bedding, T. R., Kjeldsen, H. 1995, apj, 443, L29
Galsgaard, K. 1995, A&A, (in preparation)
Galsgaard, K., Nordlund, Å. 1995a, J. Geophys. Res., (submitted)
Galsgaard, K., Nordlund, Å. 1995b, J. Geophys. Res., (in preparation)
Gigas, D., Steffen, M. 1984, Publikation der Sternwarte Kiel, 1–131
Goldreich, P., Keeley, D. A. 1977, ApJ, 212, 243
Goldreich, P., Kumar, P. 1990, ApJ, 363, 694
Graham, E. 1977, in E. A. Spiegel, J. P. Zahn (eds.), Problems of Stellar Convection, Lecture Notes in Physics 71, Springer-Verlag, Berlin, p. 151
Hossain, M., Mullan, D. J. 1990, ApJ, 354, L33
Hossain, M., Mullan, D. J. 1991, ApJ, 380, 631
Hurlburt, N. E., Brummell, N. H., Toomre, J. 1995, in The 4th SOHO Workshop: Helioseismology
Lee, T. T., Petrosian, V., McTiernan, J. M. 1993, ApJ, 412, 401
Lites, B. W., Rutten, R. J., Kalkofen, W. 1993, ApJ, 414, 345
Lu, E. T., Hamilton, R. J. 1991, ApJ, 380, l89

Lu, E. T., Hamilton, R. J., McTiernan, J. M., Bromund, K. 1993, ApJ, 412, 841

Nordlund, Å. 1982, A&A, 107, 1

Nordlund, A. 1985a, in S. Keil (ed.), Small Scale Dynamical Processes in Quiet Stellar Atmospheres, Sacramento Peak publication

Nordlund, A. 1985b, NLTE Spectral Line Formation in a Three-Dimensional Atmosphere with Velocity Fields, Vol. 152 of *NATO Advanced Science Institute Series*, 215–224, Reidel

Nordlund, Å. 1986, Solar Physics, 100, 209

Nordlund, A., Brandenburg, A., Jennings, R. L., Rieutord, M., Roukolainen, J., Stein, R. F., Touminen, I. 1992, ApJ, 392, 647

Nordlund, A., Brandenburg, A., Stein, R. F. 1996, ApJ, (in preparation)

Nordlund, Å., Dravins, D. 1990, A&A, 228, 155

Nordlund, Å., Galsgaard, K., Stein, R. F. 1994, in R. J. Rutten, C. J. Schrijver (eds.), Solar Surface Magnetic Fields, Vol. 433, NATO ASI Series

Nordlund, Å., Stein, R. F. 1990, Computer Phys. Communications, 59, 119

Nordlund, Å., Stein, R. F. 1991, in D. Gough, J. Toomre (eds.), Challenges to Theories of the Structure of Moderate Mass Stars, Vol. 388 of *Lecture Notes in Physics*, Springer, Heidelberg, p. 141

Porter, D. H., Woodward, P. R. 1994, ApJS, 93, 309

Pulkkinen, P., Touminen, I., Brandenburg, A., Nordlund, Å., Stein, R. F. 1991, in The Sun and Cool Stars: Activity, Magnetism, Dynamos, Vol. 380 of *Lecture Notes in Physics*, p. 98

Pulkkinen, P., Tuominen, I., A., B., Nordlund, Å., Stein, R. F. 1993, Astronomy and Astrophysics, 267, 265

Rast, M. P., Nordlund, Å., Stein, R. F., Toomre, J. 1993, ApJ, 408, L53

Rosenthal, C. S., Christensen-Dalsgaard, J., Houdek, G., Monteiro, M., Nordlund, A., Trampedach, R. 1995, in Proc. of 4th SOHO Workshop, Noordwijk, June 1995, (submitted)

Solanki, S., Rüedi, I., Bianda, M., Steffen, M. 1995, A&A, (submitted)

Steffen, M., Freytag, B. 1991, in G. Klare (ed.), Reviews in Modern Astronomy, Vol. 4, Springer, Heidelberg, p. 43

Steffen, M., Ludwig, H.-G., Krüss, A. 1989, A&A, 213, 371

Stein, R. F., Nordlund, Å. 1989, ApJ, 342, L95

Stein, R. F., Nordlund, Å. 1991, in D. Gough, J. Toomre (eds.), Challenges to Theories of the Structure of Moderate Mass Stars, Vol. 388 of *Lecture Notes in Physics*, Springer, Heidelberg, p. 195

Stein, R. F., Nordlund, A. 1994, in D. Rabin, J. Jefferies, C. Lindsey (eds.), Infrared Solar Physics, IAU Symposium 154, Kluwer, Dordrecht, p. 225

Stein, R. F., Nordlund, A. 1996, ApJ, (in preparation)

Toomre, J., Brummell, N., Cattaneo, F., Hurlburt, N. E. 1990, Comp. Phys. Comm., 59, 105

Trampedach, R., Christensen-Dalsgaard, J., Nordlund, A., Stein, R. F. 1996, A&A, (in preparation)